THE JOURNAL OF BIOLOGICAL CHEMISTRY VOL. 286, NO. 8, pp. 6733–6741, February 25, 2011

ATP Induces Conformational Changes in the Carboxyl-terminal Region of ClC-5*[S]

Received for publication, August 18, 2010, and in revised form, December 14, 2010 Published, JBC Papers in Press, December 20, 2010, DOI 10.1074/jbc.M110.175877

Leigh Wellhauser[‡§], Cesar Luna-Chavez[¶], Christina D'Antonio[‖], John Tainer[¶‡‡], and Christine E. Bear[‡§‖1]**

*From the [‡]Programme of Molecular Structure and Function, Research Institute, the Hospital for Sick Children, Toronto, Ontario M5G 1X8, Canada, the [§]Department of Biochemistry, Faculty of Medicine, the University of Toronto, Toronto, Ontario M5S 1A8, Canada, the [¶]Lawrence Berkeley National Library, the University of California, Berkeley, California 94720, the **Scripps Research Institute, La Jolla, California 92037 , the [‡‡]Department of Molecular Biology, the Skaggs Institute for Chemical Biology, La Jolla, California 92037, and the [‖]Department of Physiology, the University of Toronto, Toronto, Ontario M5S 1A8, Canada*

ATP binding enhances the activity of ClC-5, the transporter mutated in Dent disease, a disease affecting the renal proximal tubule. Previously, the ATP binding site was revealed in x-ray crystal structures of the cytoplasmic region of this membrane protein. Disruption of this site by mutagenesis (Y617A-ClC-5) reduced the functional expression and ATP-dependent regulation of the full-length transporter in *Xenopus* oocytes. However, insight into the conformational changes underlying ATP-dependent regulation is lacking. Here, we show that ATP binding induces a change in protein conformation. Specifically, small angle x-ray scattering experiments indicate that ATP binding promotes a clamp-like closure of the isolated ClC-5 carboxyl-terminal region. Limited proteolysis studies show that ATP binding induces conformational compaction of the carboxyl-terminal region in the intact membrane protein as well. In the context of fibroblasts and proximal tubule epithelial cells, disruption of the ATP binding site in full-length ClC-5 (Y617A-ClC-5) led to a defect in processing and trafficking out of the endoplasmic reticulum. These latter findings account for the decrease in functional expression previously reported for this ATP-binding mutant and prompt future study of a model whereby conformational compaction caused by ATP binding promotes biosynthetic maturation.

Mutations in ClC-5 cause Dent disease and renal failure in severe cases; therefore, a thorough understanding of its regulation is required for comprehending the biology and for improved management of human disease (1–3). In the proximal tubule and in recombinant expression systems, ClC-5 functions as a Cl^-/H^+ antiporter in endosomal membranes (early and recycling endosomes) and on the cell surface (4, 5). Zifarelli and Pusch recently showed in electrophysiological studies that ATP binding to the wild-type (WT) ClC-5, but not the binding mutant Y617A-ClC-5, caused a modest yet significant increase in the transporter activity of ClC-5, providing an important clue regarding the regulation of its activity (6). Interestingly, this binding mutant also conferred less total chloride flux (*i.e.* current density) on the surface of *Xenopus* oocytes (6), suggesting that ATP binding may serve multiple roles with respect to the functional expression of this transporter.

ATP binding is associated with conformational changes essential for the activity of numerous pumps, transporters, and channels (*i.e.* Na^+/K^+-ATPase) (7), vacuolar H^+-ATPase (8), P-glycoprotein (9), MsbA (10), and cystic fibrosis transmembrane conductance regulator (CFTR)[2] (11). The extensive carboxyl-terminal (Ct) region of eukaryotic ClC proteins (including ClC-5) possesses a pair of CBS domains that form an ATP binding pocket. The x-ray crystal structure of the Ct region of ClC-5 with bound ATP was solved, defining the nucleotide binding site at atomic resolution (12). However, the structure of the apo form of ClC-5 has yet to be characterized. Hence, the conformational changes induced by ATP binding to the carboxyl terminus of ClC-5 are unknown. To address this gap in our understanding, we directly assessed the local conformational changes in the Ct region upon ATP binding using small angle x-ray diffraction (SAX) and characterized the effect of this interaction on conformation of the full-length protein in membranes, using limited proteolysis. The consequences of ATP binding on protein conformation *in vivo* was evaluated in proximal tubule epithelial cells, the tissue in which ClC-5 expression is critical for renal health (1–3).

EXPERIMENTAL PROCEDURES

DNA Constructs—The ClC-5 Ct and full-length HA-ClC-5 constructs were generated as described previously (13). The pCMV6 construct containing human ClC-5 tagged at its car-

* This work was supported by a grant from the Kidney Foundation of Canada (to C. E. B.) and a postgraduate studentship from the Natural Sciences and Engineering Research Council of Canada (to L. W.). Support for advancement of SAXS technologies at the Lawrence Berkeley National Laboratory SIBYLS beamline came from the Integrated Diffraction Analysis Technologies program under Contract DE-AC02-05CH11231 with the U. S. Department of Energy.

[S] The on-line version of this article (available at http://www.jbc.org) contains supplemental Figs. 1 and 2 and Experimental Procedures.

[1] To whom correspondence should be addressed: 555 University Ave., Toronto, ON M5S 1X8, Canada. Tel.: 416-813-5981; Fax: 416-813-5028; E-mail: bear@sickkids.on.ca.

[2] The abbreviations used are: CFTR, cystic fibrosis transmembrane conductance regulator; CBS, cystathionine beta synthase; Bz-ATP, adenosine 5′-[γ-^{32}P]triphosphate [γ]benzophenone; CHO, Chinese hamster ovary; Ct, carboxyl-terminal; D_{max}, maximum dimension; ER, endoplasmic reticulum; I(q), scattering intensity; OK, opossum kidney; P(r), pairwise distribution; R_g, radius of gyration; SAX, small angle x-ray diffraction; SAXS, small-angle x-ray scattering; TMD, transmembrane domain; TNP-ATP, 2′(3′)-*O*-(2,4,6-trinitrophenyl)adenosine 5′-triphosphate.

boxyl terminus with a FLAG tag (FLAG-ClC-5) was obtained from OriGene (Rockville, MD). The open reading frame of ClC-5 (kindly provided by T. Jentsch) was introduced into the pBlueBac4 vector (Invitrogen) for generation of the HA-ClC-5 baculovirus.

Antibodies—The α-FLAG antibody was obtained from Sigma. The α-HA and Alexa Fluor 488/594-conjugated antibodies were obtained from Covance (Princeton, NJ) and Invitrogen, respectively.

Protein Purification—The ClC-5 Ct peptide (residues 575–746) was expressed and purified as described previously (13). Purified protein was dialyzed into buffer A (100 mM Tris, 500 mM NaCl, 5 mM TCEP, pH 8.0).

Small-angle X-ray Scattering (SAXS)—SAXS data were collected at the SIBYLS beamline (12.3.1) at the Advanced Light Source in the Lawrence Berkeley National Laboratory (14, 15). The incident wavelength (λ) of 1.03 Å was used with a q range of 0.01–0.35 $Å^{-1}$ ($q = 4\pi \sin(\theta/2)/\lambda$, where θ is the scattering angle), and scattering was detected by a MAR 165 CCD area detector. ClC-5 Ct peptide samples (2.5, 5.0, and 10 mg/ml) were placed in a 1-mm thick cuvette exposed to helium gas. Data sets were corrected for buffer A alone and were analyzed using PRIMUS (16) and GNOM (17) to extract the radius of gyration (R_g) according to the Guinier approximation or the POROD law, respectively (17). The molecular mass of the peptide was derived from the POROD volume (volume/2 = molecular mass) (13). The pairwise distribution, P(r), function was calculated using the indirect transformation of the scattering intensity $I(q)$ using the program GNOM upon which the protein's maximum dimension (D_{max}) was derived. The Kratky plot was generated by plotting the $q^2 \times I(q)$ across all q values.

TNP-ATP Binding Assay—TNP-ATP (0–50 μM) was incubated with ClC-5 Ct peptides (4.3 μM) in buffer A for 1 min prior to reading the fluorescence (λ_{ex} 410 nm and λ_{em} 500–600 nm) using a Photon Technology International C-60 spectrofluorometer (18). A buffer control was used to correct for the inner filter effect as described previously (19). Supplemental Fig. 2 shows TNP-ATP binding to WT ClC-5 Ct peptide.

Circular Dichroism (CD)—CD was performed on a Jasco J-810 spectropolarimeter (Jasco, Easton, MD) using Ct peptides (15 μM in 5 mM Tris, 500 mM NaCl, pH 8.0) (13).

ClC-5 Expression in Sf9 Cells—Crude membranes from Sf9 cells infected with ClC-5 baculovirus (48 h) were isolated as noted previously (20).

Photoaffinity Labeling—Crude membranes (100 μg of protein) were incubated with $MgATP^{2-}$ (1 h, 4 °C). Adenosine 5′-[γ-^{32}P]triphosphate [γ]benzophenone (Bz-ATP; Affinity Photoprobes, Lexington, KY) was incubated with the samples (50 μM, 1 h, 4 °C). Samples were exposed to ultraviolet light (5 min, 4 °C) and solubilized in modified radioimmune precipitation assay buffer (50 mM Tris-Cl, 150 mM NaCl, 1 mM EDTA, pH 7.4, 0.2% (v/v) SDS, and 0.1% (v/v) Triton-100). ClC-5 was immunoprecipitated (α-HA antibody), and samples were subjected to autoradiography and Western blotting.

Limited Proteolysis—Crude membranes (100 μg of protein) expressing either WT or Y617A ClC-5 were incubated with trypsin (0–50 μg/ml) as described previously (20).

Protein Expression in Mammalian Cells—Chinese hamster ovary (CHO) cells were transfected with HA-ClC-5 or FLAG-ClC-5 using FuGENE 6 (Roche Applied Science) according to the manufacturer's protocol 24 h after plating, and total expression was enhanced using sodium butyrate (5 mM for an additional 24 h). Temperature dependence of biosynthesis was assessed by incubating cells at 37 °C or 27 °C during the subsequent 24 h in the continued presence of sodium butyrate. Cells were treated with glycosidases according to the manufacturer's protocol (New England BioLabs).

Cell Surface Biotinylation—CHO cells were subjected to cell surface biotinylation as described previously (21). Briefly, cells were biotinylation with 1 mg/ml sulfosuccinimidyl-2-(biotinamido)-ethyl-1,3-dithiopropionate (Pierce) in biotinylation buffer (150 mM NaCl, 5 mM KCl, 1 mM $CaCl_2$, 1 mM $MgCl_2$, 20 mM HEPES, pH 7.4). Biotinylation was quenched by application of cold 1% (w/v) BSA in PBS. Cells were then lysed with radioimmune precipitation assay buffer, and cell extracts were collected by centrifugation (15,000 × g, 10 min). Supernatants were incubated with streptavidin beads (Pierce) for 1 h at 4 °C and biotinylated proteins were eluted from beads with SDS sample buffer (63 mM Tris, pH 6.8, 10% (v/v) glycerol, 0.5 mM EDTA, 2% (w/v) SDS, 2% (v/v) β-mercaptoethanol, and 50 mM DTT) at 59 °C. Samples were analyzed by SDS-PAGE and Western blotting using the α-HA or α-actin antibody to determine the ratio of the biotinylated ClC-5 (surface levels) relative to its total cellular expression.

Epithelial Cell Biology—Opossum kidney epithelial (OK) cells, a well established model of the kidney proximal tubule (22), were obtained from the American Type Culture Collection (ATCC) and were propagated in DMEM (Wisent) supplemented with 10% FBS (Wisent). OK cells were maintained at 37 °C with 5% CO_2 and 95% O_2. As in the case of the CHO cell studies, OK cells were transiently transfected with ClC-5 cDNA, a gift from Dr. T. J. Jentsch, after being subcloned into a pcDNA3.1 vector. A HA tag was inserted onto the amino terminus of ClC-5 for subsequent identification of ClC-5 proteins. Unless stated otherwise, cells were treated with 5 mM sodium butyrate over the 24-h transfection period to enhance ClC-5 protein expression.

Immunofluorescence and Confocal Microscopy—Immunofluorescence labeling was performed as described previously (23, 24). The following primary antibodies were used: mouse anti-HA antibody to detect HA-ClC-5 or HA-Y617A-ClC-5 and rabbit anti-calnexin antibody to detect this endoplasmic reticulum (ER)-resident protein. An Alexa Fluor 488 goat anti-mouse antibody was used to visualize ClC-5 proteins, whereas a rhodamine goat anti-rabbit antibody was employed to visualize calnexin (Molecular Probes).

Immunofluorescence images were acquired using a Quorum Spinning Disk Confocal Microscope (Leica DMIRE2 inverted fluorescence microscope equipped with a Hamamtsu Black-thinned EM-CCD camera and spinning disk confocal head) (Leica Microsystems) (Hamamtsu Photonics). Alexa Fluor 488 (green) and rhodamine (red) fluorophores were excited with a 491-nm and a 561-nm diode-pumped solid-state laser lines, respectively. A 63× objective was utilized to visualize all samples. The spinning disk confocal microscope

system was driven by Volocity acquisition software. Z-stacks were acquired for each of the red and green channels, capturing 0.2-μm slices that together encompassed the entire depth of the cells. The fluorescent confocal images depicted are a single 0.2 μM slice, taken at the cell midsection.

Size-exclusion Chromatography—Size-exclusion chromatography is described in supplemental Experimental Procedures.

Quantification and Statistics—Pixel intensity of Western blots and autoradiographs was quantified using ImageJ, and all data are shown as mean ± S.E. Statistical analyses were conducted using Prism 4 software (GraphPad, San Diego, CA).

RESULTS

Isolated Ct Region of ClC-5 (ClC-5-Ct) Undergoes Conformational Compaction upon ATP Binding—Although a structural model of ATP-bound ClC-5 Ct region exists, the unbound structure is unknown (12). To capture dynamic, nucleotide-dependent conformational changes in the ClC-5 Ct peptide, we employed SAXS, which provides an objective, quantitative measure of structural shape and assembly in solution (14, 15). We used SAXS to examine the purified ClC-5 Ct peptide (residues 575–746) in solution and changes resulting from ATP binding. Not surprisingly, given the dimeric structure of bacterial ClC proteins and the red algae ClC protein (25, 26), the Ct regions of eukaryotic family members exhibit a propensity for dimerization (27, 28). Previous studies suggested that the Ct domain of ClC-5 exists in a monomer-dimer equilibrium, insensitive to addition of nucleotides (12), and our results confirmed these findings. Size exclusion chromatography identified the predominant species as ClC-5 Ct monomers and dimers with the relative distribution maintained upon addition of ATP (supplemental Fig. 1). The absence of an ATP-dependent effect on the monomer:dimer ratio is consistent with the model proposed by Meyer *et al.* wherein the nucleotide binding site faces away from the dimer interface (12). Because the quaternary structure of the isolated Ct region of ClC-5 was not affected by nucleotide addition, we employed SAXS to evaluate ATP-dependent conformational changes directly. We focused on ATP in the current work because it is the most abundant of the adenine nucleotides in the cell, and previous studies argue that the binding site on ClC-5 does not discriminate among ATP, ADP, and AMP with respect to binding affinity (6, 12).

SAXS scattering curves (Fig. 1*A*) and derived structural parameters, including molecular mass, R_g, and D_{max}, are summarized in Table 1. The 39.6-kDa global molecular mass determined by SAXS is close to the ~42 kDa prediction from sequence for the Ct dimer. SAXS simulation based upon the Ct dimer identified in the crystal structure (A/B pair, Protein Data Bank ID code 2J9L) produced a theoretical R_g (22.7 Å) significantly smaller than the experimental R_g value found here (34.5 ± 0.07 Å). An elongated structure in solution is also supported by the shape of the $P(r)$ function, which exhibits an asymmetric profile typical of an elongated protein (Fig. 1*C*). In particular, the plot possesses a peak at ~r = 25 Å, a shoulder at ~r = 40 Å, and a long falling edge extending to larger r values (29, 30).

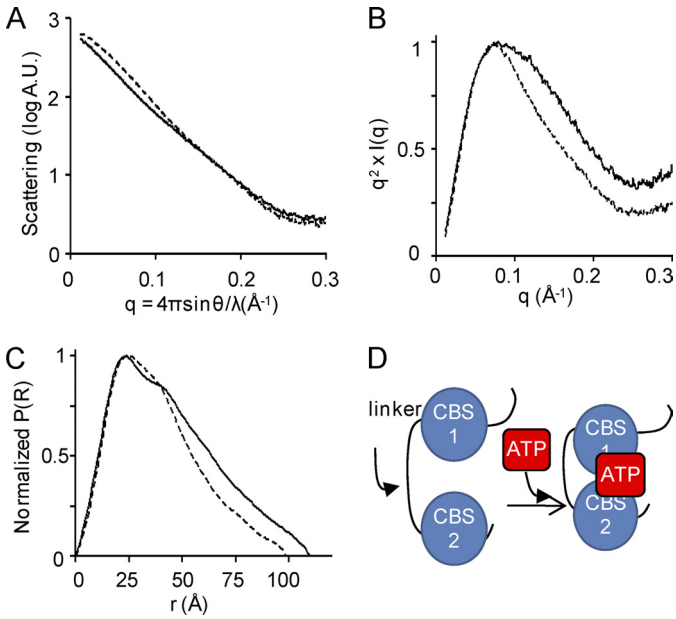

FIGURE 1. **ATP binding induces a conformational change in the ClC-5 Ct region.** All SAXS experiments were performed on 400 μM ClC-5 Ct peptide in 100 mM Tris, 500 mM NaCl, 5 mM TCEP, pH 8.0, with and without 5 mM ATP. Three independent trials were preformed on separate protein batches, and a representative experiment is shown in *A–D*. *A*, SAXS profiles of apo (*solid line*) or ATP-bound (*dotted line*) ClC-5 Ct peptide. *B*, normalized pairwise distribution functions for apo (*solid line*) and ATP-bound (*dotted line*) ClC-5 Ct peptide. *C*, Kratky plot of apo (*solid line*) or ATP-bound (*dotted line*) ClC-5 Ct peptide. *D*, proposed model of the clamp-like motion of ClC-5 CBS domains around the ATP molecule.

TABLE 1
Structural parameter of ClC-5 Ct derived from SAXS

Ct	Average molecular mass	R_g	D_{max}	Volume
	kDa	*Å*	*Å*	*Å^3*
Apo Ct	39.6	34.5 ± 0.07	110 ± 5.0	19.8 ± 4.9
+ ATP	31.1	29.9 ± 0.10	100 ± 5.0	14.4 ± 2.7

SAXS objectively measures folding such that Kratky plots, $q^2 \times I(q)$ *versus* q, are parabolic for folded structures, asymptotic for unfolded structures, and intermediate for partially folded structures (14). Consistent with a partly flexible or extended Ct domain, the Kratky plot (Fig. 1*B*), shows the intermediate, partly parabolic curve with sharp maximum followed by an up-swung tail, the hallmark of a partially folded domain with flexible or extended region(s) (30, 31). The loop (~30 residues) connecting the two CBS domains in ClC-5 exhibits a high propensity for disorder as predicted using DRIPRED and may contribute to the dynamics detected by SAXS.

We next repeated SAXS on the ClC-5 Ct peptide in the presence of 5 mM ATP (Fig. 1*A*). ATP binding promoted a significant decrease in the peptide R_g and D_{max} and peptide volume (Table 1). These parameters reveal a globally more compact ClC-5 Ct peptide upon ATP binding. This finding is also supported by the shape of the $P(r)$ function, which exhibits a less pronounced shoulder at ~40 Å in the presence of ATP, suggesting that the protein is becoming less modular (Fig. 1*C*). Interestingly, the overall shape of the Kratky plot

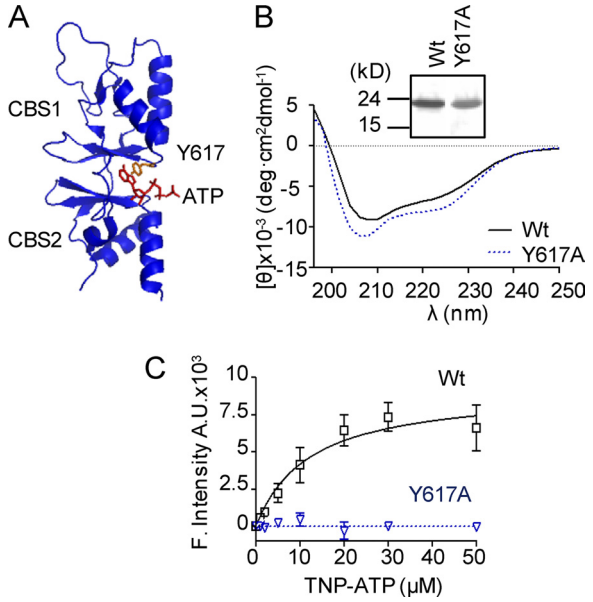

FIGURE 2. **ATP binding to the ClC-5 Ct peptide is impaired by the Y617A mutation.** *A*, interaction with Tyr-617 of ClC-5 Ct peptide (Protein Data Bank ID code 2J9L) with ATP, essential for its binding and co-ordination (10). *B*, CD spectra of WT and mutant (Y617A) Ct peptides (15 μM each in 5 mM Tris, 500 mM NaCl, pH 8.0). *Inset* represents silver-stained SDS-PAGE of purified proteins. *C*, concentration curve of TNP-ATP binding by WT (*squares*) and Y617A (*triangles*) Ct peptides (4.3 μM) from 0 to 50 μM TNP-ATP. The K_d for WT Ct peptide is 11.87 ± 5.1 μM TNP-ATP (n = 4 trials each).

(Fig. 1*B*) does not change in the presence of ATP, indicating that the dynamic regions of ClC-5 Ct peptide are not ordered upon binding of nucleotides. This result is consistent with the lack of secondary structural changes induced upon ATP binding reported previously (13). Collectively, these findings support a model wherein there is a "clamp-like" closure of the CBS domains around the bound nucleotide (Fig. 1*D*). A similar conformational change has also been reported upon nucleotide binding to unrelated pairs of CBS domains (32, 33).

The SAX studies support a model wherein the Ct region of ClC-5 clamps around ATP to form a more compact structure. These findings support and extend our previous studies using CD spectroscopy, where we showed that the isolated ClC-5 Ct region becomes more thermally stable when directly bound with ATP (13).

Mutagenesis of the ATP Binding Site in the Isolated ClC-5 Ct Region Leads to Decreased Thermal Stability—We mutated the tyrosine residue which interacts with ATP in the x-ray crystal structure (Fig. 2 *A*) (12) to confirm that the conformational changes detected in the previous experiments were induced by binding to this site. The isolated ClC-5 Ct protein carrying the Y617A substitution was expressed in *Escherichia coli* and purified as shown in Fig. 2*B*. Importantly, the Y617A mutation did not significantly alter the secondary structure relative to WT protein as determined in CD studies. (Fig. 2*B*).

First, we confirmed the role for Tyr-617 in ATP binding to ClC-5 Ct. In these studies, we employed the ATP analog, TNP-ATP, which fluoresces upon binding to hydrophobic nucleotide binding pockets (34) (supplemental Fig. 2*A*). The concentration dependence of TNP-ATP binding to WT ClC-5 Ct peptide (Fig. 2*C*) showed saturable binding with an affinity of ~10 μM. Despite this relatively high affinity, TNP-

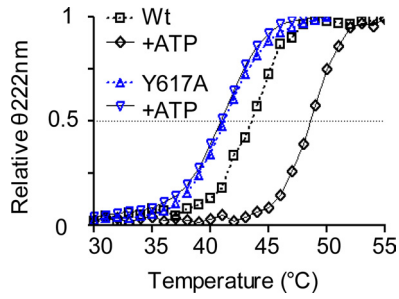

FIGURE 3. **Y617A ClC-5 Ct mutant is thermally unstable.** Thermal melts of purified WT (11) and Y617A Ct peptides (15 μM) ± 500 μM ATP was monitored by $\theta_{222\ nm}$. The T_m values for WT protein (apo = 44.16 ± 0.82 and +ATP = 48.95 ± 0.24 °C, p = 0.001 (11) and Y617A protein (apo = 41.15 ± 0.08 and +ATP 41.37 ± 0.12 °C, p = 0.205) were measured.

ATP binding to WTClC-5 Ct protein and resulting fluorescence could be competed by the natural ligand, ATP (supplemental Fig. 2*B*). On the other hand, addition of TNP-ATP to the same quantity of Y617A ClC-5 Ct mutant protein failed to lead to a measurable change in fluorescence (Fig. 2*C*). Hence, as predicted by Meyer and colleagues (12), the Y617A mutation disrupted nucleotide binding in the context of the isolated ClC-5 Ct region.

Previously, we found that in CD studies the WT ClC-5 Ct region becomes more thermally stable when bound with nucleotides (13). Because the Y617A protein fails to bind ATP, we reasoned that it would fail to show an increase in thermal stability upon ATP addition. As we predicted, the addition of 500 μM ATP did not significantly increase the T_m value for Y617A Ct peptide (Fig. 3; apo = 41.15 ± 0.08 °C and +ATP = 41.37 ± 0.12 °C, respectively (p = 0.205) unlike WT Ct protein (Fig. 3; apo = 44.16 ± 0.82 °C and +ATP = 48.95 ± 0.24 °C, *, p = 0.001) (13). It should be noted that the unbound Y617A Ct peptide was less thermally stable than WT protein (T_m values of 41.15 ± 0.08 °C and 44.16 ± 0.82 °C, respectively). The increased susceptibility of the Y617A mutant to thermal denaturation is not due to a loss of secondary structure but could possibly arise from the loss of a buried hydrophobic side chain and creation of a solvent-accessible cavity upon mutation of a tyrosine to an alanine residue. The relative instability of this protein prevented detailed analysis using SAX methods.

Tyrosine 617 Comprises the ATP Binding Site on the Full-length ClC-5 Protein Expressed in Sf9 Cells—Direct ATP binding to full-length ClC-5 was assessed using the photoreactive ATP analog Bz-ATP. For this purpose, the full-length ClC-5 protein was expressed in Sf9 cells using the baculovirus system to ensure high levels of expression. In contrast to its expression in mammalian cells (refer to Fig. 6 showing expression of multiple bands), the full-length ClC-5 protein produced in Sf9 cells migrates as a single 76-kDa protein (Fig. 4). This observation is consistent with previous reports showing that very little processing of the high mannose oligosaccharide core occurs in these cells (35). As shown in Fig. 4*A*, labeling of ClC-5 with Bz-ATP was competed by preincubation of the membranes with $MgATP^{2-}$ with a half-maximal competition observed at 1.28 ± 0.17 mM ATP (r^2 = 0.99). These results ensured that Bz-ATP photolabeling of ClC-5 was specific.

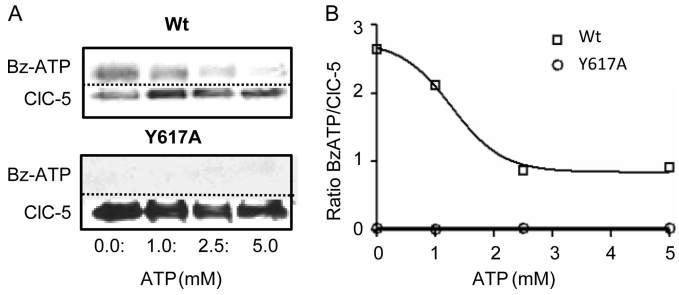

FIGURE 4. **Full-length ClC-5 in Sf9 insect cell membranes binds ATP directly.** *A*, photoaffinity labeling of WT or Y617A ClC-5 in Sf9 membrane vesicles (100 μg of total protein) with 50 μM radioactive Bz-ATP without and with $MgATP^{2-}$ (1–5.0 mM). Following labeling ClC-5 was solubilized, and protein was immunoprecipitated (α-HA) and separated on SDS-PAGE and transferred to nitrocellulose. The nitrocellulose was probed using Western blotting (α-HA) to determine the amount of protein present and exposed to autoradiograph film to determine the amount of Bz-ATP labeling. *B*, quantification of the labeling (autoradiograph) signal *versus* protein (Western) measured using densitometry (ImageJ). The data obtained for WT ClC-5 (*squares*) was fitted to a competitive binding algorithm ($IC_{50} = 1.28 \pm 0.171$ mM ATP, $r^2 = 0.99$). No radioactive labeling was detected for Y617A ClC-5 despite abundant protein present.

We next assessed the photolabeling of full-length ClC-5 bearing the Y617A mutation. Unlike WT protein, photolabeling of Y617A ClC-5 was not observed (Fig. 4, *A* and *B*). Importantly, the defect in Bz-ATP labeling of this mutant protein was not due to its gross misfolding in Sf9 cell membranes as assessed on the basis of its WT susceptibility to trypsin proteolysis (data not shown) and consistent with its ability to mediate measurable ion conduction in other studies using nonmammalian over expression systems such as *Xenopus* oocytes (6). Therefore, these studies show that ATP binds specifically to full-length ClC-5 at the site previously identified using x-ray crystallography (12).

ATP Binding Induces Conformational Compactness in Full-length ClC-5 Protein, and Abrogation of Binding Impairs Biosynthetic Processing in Mammalian Cells—Conformational changes in full-length ClC-5 in response to ATP binding were assessed as changes in trypsin susceptibility. These experiments were performed on mammalian membranes expressing WT ClC-5 protein possessing a FLAG tag at its carboxyl terminus (ClC-5-FLAG). Upon exposure of crude membrane vesicles to low trypsin concentrations (on both sides of the membrane), a dominant fragment was generated from the full-length ClC-5-FLAG protein. This 40-kDa fragment was detected using an anti-FLAG antibody and hence was derived from the Ct region (Fig. 5 *A*). Using alignments of ClC-5 with the *E. coli*. ClC and the red algae ClC, *i.e.* (*Cyanidioschyzon merolae*) ClC (25, 26), we predicted that trypsin cleaves within the loop connecting transmembrane helices L and M (Fig. 5*C*). Preincubation of membranes with 5 mM ATP (but not 5 mM GTP, a nucleotide that was shown previously not to bind the Ct peptide (12), prior to digestion led to a dramatic reduction in the appearance of this band (Fig. 5*B*). These results are intriguing and suggest several possible scenarios. For instance, ATP binding may decrease the accessibility of the Ct FLAG tag by triggering a tighter association of the Ct region with the membrane domain distal to the trypsin cut site. Alternatively, compaction of the Ct region caused by ATP binding may bury the FLAG epitope within the Ct structure. In either case, these results suggest that ATP-dependent conformational compaction occurs not only in the isolated ClC-5 Ct peptide in solution, as reported in our SAXS studies, but is also conserved in the intact membrane protein.

We were then prompted to determine whether this ATP-dependent compaction in ClC-5 contributes to its conformational maturation during biosynthesis in mammalian cells. For many membrane proteins, including CFTR (36), mutations that prevent acquisition of normal conformation (*i.e.* F508del-CFTR) cause full or partial retention in the ER and failure to be processed by the Golgi during biosynthesis. Partial retention in the ER may account for the reduction in chloride current, or current density, conferred by Y617A-ClC-5 relative to WT ClC-5 as reported previously by Zifarelli and Pusch (6).

It is well established that WT ClC-5 protein is expressed as a complex of differentially glycosylated species when expressed in mammalian cells (37). The larger molecular mass bands (migrating as a 90–100 kDa band) are resistant to endoglycosidase H and sensitive to *N*-glycosidase F cleavage as expected for the fully processed protein (Fig. 6*A*). A fraction of the complex glycosylated form of WT ClC-5 is trafficked to the plasma membrane as revealed by cell surface biotinylation (Fig. 6, *B* and *C*). In contrast, the ATP-binding mutant (Y617A-ClC-5) was not efficiently glycosylated nor properly trafficked to the cell surface, a phenotype consistent with conformational instability and ER retention (36, 37) (Fig. 6, *B* and *C*).

We also examined the consequences of disrupting the ATP binding site in ClC-5 on its trafficking in the OK cell line because this cell line models the proximal tubule epithelium, the tissue in which ClC-5 expression is physiologically relevant (37–39). As shown in Fig. 7, the defect in biosynthetic processing observed for the ATP-binding mutant Y617A-ClC-5 expressed in CHO cells is also evident in OK cells. Confocal micrographs of OK cells expressing either WT ClC-5 or Y617-ClC-5 reveal differential cellular localization. Unlike WT-ClC-5, which exhibits expression both in the ER (localized by labeling calnexin protein) and in discrete puncta (identified as early endosomes in previous publications) (40), Y617-ClC-5 is localized predominantly in the ER, colocalized with calnexin and is largely excluded from these puncta (Fig. 7).

DISCUSSION

A role for ATP binding in inducing changes in conformation and activity is well documented for a wide variety of membrane proteins, including pumps, transporters, and channels. Prior to the current report, little was known concerning the impact of ATP on the structure of the ClC-5 protein despite evidence to support a role for nucleotides in its functional regulation (6). Here, we provide the first evidence of ATP-dependent structural changes in the human ClC family of channels and transporters. Specifically, we demonstrate that ATP binding to the Ct region of ClC-5 protein enhances its global compactness and increases its thermal stability, likely by inducing a "clamp-like" closure of its CBS domains. We reason that this structural change in the isolated Ct re-

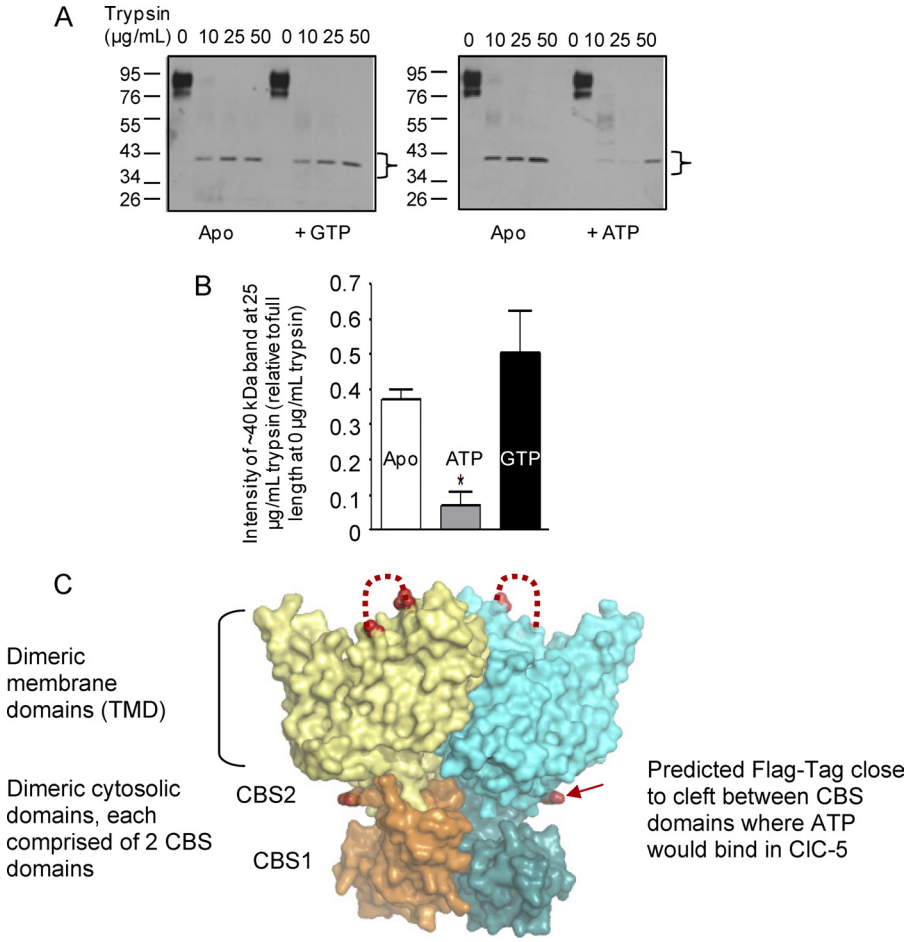

FIGURE 5. **ATP binding reduces trypsin susceptibility of Ct region in WT, full-length ClC-5 protein.** *A*, Western blots (α-FLAG) of WT ClC-5 (100 μg of total protein), containing a Ct FLAG tag, incubated without and with 5 mM GTP or ATP for 1 h prior to being subjected to limited trypsin (0–50 μg/ml) proteolysis for 15 min at 4 °C. Representative blots for each condition are shown, and the ~40 kDa band quantified in *B* is indicated by a *bracket*. *B*, *bar graph* of trypsin susceptibility of ClC-5 without and with the presence (*Apo*; *open bar*) of 5 mM GTP (*black filled bar*) or ATP (*gray filled bar*). Specifically, the intensity of the ~40 kDa band (detected by the α-FLAG antibody) at 25 μg/ml trypsin was quantified for each condition using ImageJ. The abundance of the ~40 kDa band generated from untreated ClC-5 membranes (0.37 ± 0.03 arbitrary units; $n = 4$) or membranes treated with GTP (0.50 ± 0.12 arbitrary units; $n = 3$) was significantly higher than the band intensity generated in the presence of ATP (0.07 ± 0.12, $n = 3$) at 25 μg/ml trypsin (*, $p = 0.001$ (*versus* apo) and $p = 0.0164$ (*versus* GTP)). *C*, size of the proteolytic product of ~40 kDa in size indicates that trypsin likely cuts ClC-5 in the loop connecting transmembrane α-helices L and M as *highlighted* (*red stippled line*) on the structure of *C. merolae* ClC (Cm-ClC, a eukaryotic ortholog, aligned with ClC-5 by Feng *et al.* (26), Protein Data Bank ID code 3ORG). Three putative trypsin sites lie in this loop in ClC-5 as predicted by ExPASy. Cm-ClC provides a model for ClC-5. Cm-ClC is a homodimer, with each monomer possessing a TMD and a cytosolic domain with two CBS domains. The extreme carboxyl terminus of Cm-ClC after truncation by seven residues is shown using a *red arrow*. This terminus lies close to the cleft between the CBS domains, the cleft to which ATP binds in ClC-5 and the membrane domain (12). This image was generated using PyMOL (DeLano Scientific LLC).

gion is recapitulated in the context of the full-length ClC-5 protein in the presence of ATP. These conformational changes likely underlie, at least in part, the mechanism for nucleotide-dependent regulation of ClC-5 antiporter activity previously reported by Zifarelli and Pusch (6).

The formation of specific molecular contacts between the CBS domains and ATP, as identified by x-ray crystallography (12), likely mediates the clamping motion of these domains around the nucleotide. This movement, which is evident upon the reduced R_g and modularity of the Ct region reported here by SAXS experiments, all in the absence of any secondary structural changes reported previously (13), is likely partially responsible for the enhanced thermal stability of the Ct region when bound with ATP. Furthermore, bridging of the CBS domains through the extensive array of contacts mediated by the nucleotide moiety likely also increases the energy of stabilization of this protein region. Upon closure of the cleft and reduction of conformational flexibility, solvent access to the interior of the protein is reduced, and the melting temperature is increased. Intriguingly, positively charged residues from both CBS1 (Arg-638, Arg-637) and CBS2 (Arg-709, Lys-725) surround the negative γ-phosphate of ATP. Although these residues do not make notable contact with this phosphate group in the x-ray crystal structure (Protein Data Bank ID code 2J9L), a minor conformational change toward a more compact CBS dimer would enable the formation of electrostatic interactions to stabilize this conformation and further occlude solvent.

It is currently unknown how conformational changes induced upon nucleotide binding to the Ct region can enhance the antiporter activity of ClC-5, as reported by Zifarelli and Pusch (6). ATP binding and neutralization of the positive cluster (defined in the preceding paragraph) by the negative phosphate moieties may subsequently modify how this region

interacts with the membrane domain. In turn, downstream movements in transmembrane helices may underlie changes in ClC-5-mediated ion translocation. In fact, helical movements coinciding with ClC activation have been described previously for the terminal membrane helix (R helix) of related proteins: ClC-0 and ClC-ec (41, 42). The orientation of the R helix in the membrane could be altered in response to ATP binding to the Ct domain thereby modifying the ion conduction pathway, as suggested by Meyer and colleagues (12). The results of our protease susceptibility studies are consistent with this idea. For instance, the Ct FLAG epitope on a fragment encompassing helical segments M through R plus the entire carboxyl terminus is more stably buried following ATP binding. We speculate that the FLAG tag may be buried at the interface between these distal helical segments (M–R) and the compact Ct region after ATP binding (Fig. 7). Interestingly, He and colleagues described such a functional interaction between the Ct region and the membrane domain of the *Caenorhabditis elegans* channel, CLH-3b (43). The recent crystal structure of the eukaryotic (*Cyanidioschyzon merolae*) ClC (Cm-ClC), shows that the CBS domains directly interact with the transmembrane domain (TMD) and further that the extreme carboxyl terminus contributes to the TMD and CBS interface (26). Future experiments are required to confirm the relevance of the Cm-ClC structure to our understanding of structure: function relationships in ClC-5.

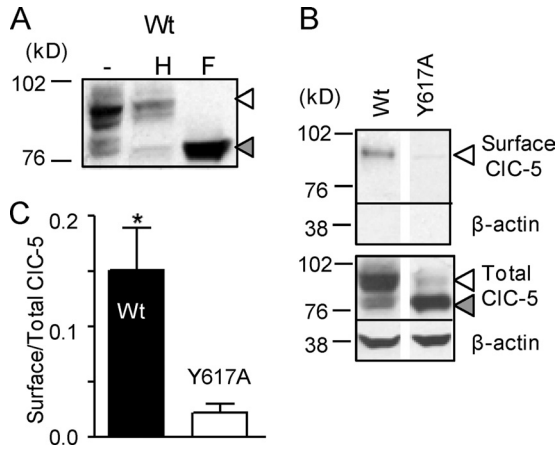

FIGURE 6. **Y617A ClC-5 mutant is misprocessed in mammalian cells.** *A*, WT ClC-5 protein expressed in CHO cells was treated with endoglycosidase H (*H*) or *N*-glycosidase F (*F*). Both a complex glycosylated (90–100-kDa proteins, *white triangle*) and core glycosylated (76–80 kDa, *gray triangle*) forms are observed. *B* and *C*, cell surface biotinylation of WT and Y617A ClC-5 in CHO cells is shown as is quantification of mean pixel intensity of surface *versus* total ClC-5 expression for WT and Y617A (0.15 ± 0.04, $n = 5$ and 0.02 ± 0.01, $n = 3$ surface/total respectively, *, $p = 0.005$). The fidelity of the biotinylation reaction in labeling cell surface expressed rather than intracellular proteins was confirmed as the lack of actin biotinylation (*B*, *top panel*).

Overall, the structural evidence reported here provides the first insight into the conformational changes induced in a ClC protein by adenine nucleotides. We speculate that enhanced compactness of the CBS dimer upon binding nucleotides is sensed by the transmembrane helices comprising the membrane domain. We speculate on the basis of the Cm-ClC structure and the results of our limited proteolysis studies that ATP binding to the CBS domains would modify domain-domain interactions in the full-length ClC-5 (Fig. 8). Further, we propose that conformational changes identified here may constitute a conserved mechanism underlying ATP-dependent regulation of eukaryotic ClC proteins possessing these domains.

Mutations causing defects in interactions that impact local stability, and hence subsequent long range conformational changes are a hallmark of single site mutations associated with many genetic diseases. Examples include defects in the xeroderma pigmentosum group D helicase that acts in nucleotide excision repair (44) and the reactive oxygen control enzyme superoxide dismutase (45), where interaction defects cause the rapidly progressing and fatal neurodegenerative disorder familial amyotrophic lateral sclerosis. Similarly, the importance of ATP binding in increasing overall compactness

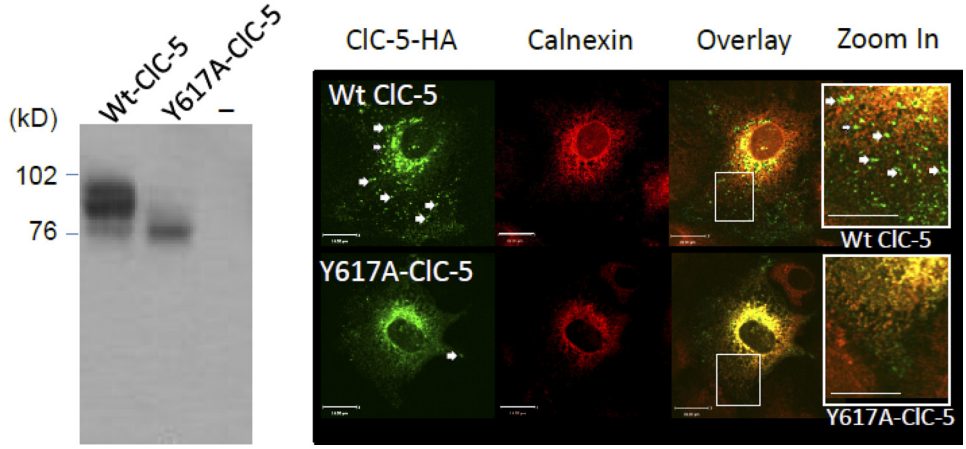

FIGURE 7. **ATP-binding mutant (Y617A-ClC-5) exhibits misprocessing and mistrafficking in proximal tubule epithelial cells.** *Left panel* shows immunoblot of lysates from OK cells expressing WT-ClC-5, Y617A-ClC-5 (each bearing an amino-terminal HA tag) or untransfected (−) and subjected to analysis by SDS-PAGE. The *upper band* indicates complex glycosylated Wt ClC-5 and *the lower band*, core glycosylated ClC-5 in both Wt-ClC-5 and Y617A-ClC-5. The confocal micrographs show the relative localization of recombinant Wt ClC-5 in the *upper panel* and Y617A-ClC-5 in the *lower panel* (labeled *green*). Cells were also labeled using an anti-calnexin antibody (*red* images). *Zoom-in* of the area defined using the *white box* in the *overlay* of the two stains revealed a distinct expression pattern for the two different proteins. WT ClC-5 in the biosynthetic compartment co-localizes with calnexin, but there is also Wt ClC-5 protein outside of the ER, expressed in punctate structures. On the other hand, the Y617A-ClC-5 expression pattern overlaps almost completely with that of calnexin. These images are representative of 82 and 66 images for each of the WT and Y617A genotypes, respectively. The *scale bars* represent 16 μm in the *three images* on the *left* and 10 μm for the *zoomed in image* on the *far right*.

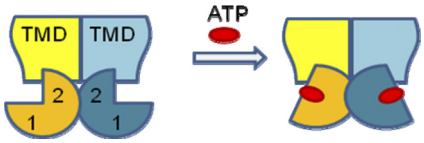

FIGURE 8. **Model of ATP-dependent conformational change in full-length ClC-5.** Enhanced global compactness of the intracellular Ct region of ClC-5 upon ATP binding is shown. The conformational compactness induced by ATP binding to the Ct regions (*pie shapes*, labeled *1* and *2* to denote CBS1 and CBS2 domains, as shown in our biochemical studies). This compactness of the Ct is also associated with its enhanced interaction with the TMD as suggested in trypsin susceptibility studies. We speculate that this large scale conformational change contributes to the activation of its transporter function as documented previously by Zifarelli and Pusch (6) and its biosynthetic processing as shown in the current paper.

is evident in structural studies of secretion ATPases (46). With respect to the current studies of ClC-5, we speculate that ATP-induced compactness exerts a positive effect on forward trafficking out of the ER. The molecular mechanisms whereby such compactness promotes anterograde trafficking to the Golgi (and/or prevents retrograde trafficking back to the ER) have yet to be defined and will constitute the focus of our future work.

Recently, it has been shown that several disease-causing mutations in ClC-5, distributed throughout the membrane domain as well as the Ct region of ClC-5 cause ClC-5 ER retention in mammalian cells. These observations suggest that there are likely to be multiple conformational checkpoints, in addition to compaction of the carboxyl terminus mediated by ATP binding, which determine exit of ClC-5 from the ER (37). Future study of the relative significance of such checkpoints in biosynthetic trafficking of ClC-5 may also have an impact on understanding the regulated biosynthesis of other members of this family. Interestingly, as in the case of the ATP binding mutant (Y617A-ClC-5) described in the current paper, a mutation in ClC-7 which causes osteopetrosis (47) leads to ER retention while it retains its function as an antiporter, pointing to the exquisite sensitivity of the ER quality control in detecting conformational abnormalities.

Acknowledgment—We thank Greg Hura for aiding the SAXS experiments.

REFERENCES

1. Lloyd, S. E., Pearce, S. H., Fisher, S. E., Steinmeyer, K., Schwappach, B., Scheinman, S. J., Harding, B., Bolino, A., Devoto, M., Goodyer, P., Rigden, S. P., Wrong, O., Jentsch, T. J., Craig, I. W., and Thakker, R. V. (1996) *Nature* **379,** 445–449
2. Lloyd, S. E., Gunther, W., Pearce, S. H., Thomson, A., Bianchi, M. L., Bosio, M., Craig, I. W., Fisher, S. E., Scheinman, S. J., Wrong, O., Jentsch, T. J., and Thakker, R. V. (1997) *Hum. Mol. Genet.* **6,** 1233–1239
3. Wrong, O. M., Norden, A. G., and Feest, T. G. (1994) *Q. J. Med.* **87,** 473–493
4. Scheel, O., Zdebik, A. A., Lourdel, S., and Jentsch, T. J. (2005) *Nature* **436,** 424–427
5. Picollo, A., and Pusch, M. (2005) *Nature* **436,** 420–423
6. Zifarelli, G., and Pusch, M. (2009) *EMBO Rep.* **10,** 1111–1116
7. Hilge, M., Siegal, G., Vuister, G. W., Güntert, P., Gloor, S. M., and Abrahams, J. P. (2003) *Nat. Struct. Biol.* **10,** 468–474
8. Landolt-Marticorena, C., Kahr, W. H., Zawarinski, P., Correa, J., and Manolson, M. F. (1999) *J. Biol. Chem.* **274,** 26057–26064
9. Senior, A. E., al-Shawi, M. K., and Urbatsch, I. L. (1995) *FEBS Lett.* **377,** 285–289
10. Borbat, P. P., Surendhran, K., Bortolus, M., Zou, P., Freed, J. H., and Mchaourab, H. S. (2007) *PLoS Biol.* **5,** e271
11. Gadsby, D. C., Vergani, P., and Csanády, L. (2006) *Nature* **440,** 477–483
12. Meyer, S., Savaresi, S., Forster, I. C., and Dutzler, R. (2007) *Nat. Struct. Mol. Biol.* **14,** 60–67
13. Wellhauser, L., Kuo, H. H., Stratford, F. L., Ramjeesingh, M., Huan, L. J., Luong, W., Li, C., Deber, C. M., and Bear, C. E. (2006) *Biochem. J.* **398,** 289–294
14. Putnam, C. D., Hammel, M., Hura, G. L., and Tainer, J. A. (2007) *Q. Rev. Biophys.* **40,** 191–285
15. Hura, G. L., Menon, A. L., Hammel, M., Rambo, R. P., Poole, F. L., 2nd, Tsutakawa, S. E., Jenney, F. E., Jr., Classen, S., Frankel, K. A., Hopkins, R. C., Yang, S. J., Scott, J. W., Dillard, B. D., Adams, M. W., and Tainer, J. A. (2009) *Nat. Methods* **6,** 606–612
16. Konarev, P. V., Volkov, V. V., Sokolova, A. V., Koch, M. H., and Svergun, D. I. (2003) *J. Appl. Crystallogr.* **36,** 1277–1282
17. Svergun, D. I. (1992) *J. Appl. Crystallogr.* **80,** 495–503
18. Stratford, F. L., Ramjeesingh, M., Cheung, J. C., Huan, L. J., and Bear, C. E. (2007) *Biochem. J.* **401,** 581–586
19. Garboczi, D. N., Thomas, P. J., and Pedersen, P. L. (1990) *J. Biol. Chem.* **265,** 14632–14637
20. Wellhauser, L., Kim Chiaw, P., Pasyk, S., Li, C., Ramjeesingh, M., and Bear, C. E. (2009) *Mol. Pharmacol.* **75,** 1430–1438
21. Dhani, S. U., Mohammad-Panah, R., Ahmed, N., Ackerley, C., Ramjeesingh, M., and Bear, C. E. (2003) *J. Biol. Chem.* **278,** 16262–16270
22. Drumm, K., Gassner, B., Silbernagl, S., and Gekle, M. (2001) *Eur. J. Med. Res.* **6,** 422–432
23. Mohammad-Panah, R., Harrison, R., Dhani, S., Ackerley, C., Huan, L. J., Wang, Y., and Bear, C. E. (2003) *J. Biol. Chem.* **278,** 29267–29277
24. Mohammad-Panah, R., Wellhauser, L., Steinberg, B. E., Wang, Y., Huan, L. J., Liu, X. D., and Bear, C. E. (2009) *J. Cell Sci.* **122,** 1229–1237
25. Dutzler, R., Campbell, E. B., Cadene, M., Chait, B. T., and MacKinnon, R. (2002) *Nature* **415,** 287–294
26. Feng, L., Campbell, E. B., Hsiung, Y., and MacKinnon, R. (2010) *Science* **330,** 635–641
27. Meyer, S., and Dutzler, R. (2006) *Structure* **14,** 299–307
28. Markovic, S., and Dutzler, R. (2007) *Structure* **15,** 715–725
29. Bernocco, S., Steiglitz, B. M., Svergun, D. I., Petoukhov, M. V., Ruggiero, F., Ricard-Blum, S., Ebel, C., Geourjon, C., Deleage, G., Font, B., Eichenberger, D., Greenspan, D. S., and Hulmes, D. J. (2003) *J. Biol. Chem.* **278,** 7199–7205
30. Moncoq, K., Broutin, I., Craescu, C. T., Vachette, P., Ducruix, A., and Durand, D. (2004) *Biophys. J.* **87,** 4056–4064
31. Segel, D. J., Eliezer, D., Uversky, V., Fink, A. L., Hodgson, K. O., and Doniach, S. (1999) *Biochemistry* **38,** 15352–15359
32. Riek, U., Scholz, R., Konarev, P., Rufer, A., Suter, M., Nazabal, A., Ringler, P., Chami, M., Müller, S. A., Neumann, D., Forstner, M., Hennig, M., Zenobi, R., Engel, A., Svergun, D., Schlattner, U., and Wallimann, T. (2008) *J. Biol. Chem.* **283,** 18331–18343
33. Lucas, M., Kortazar, D., Astigarraga, E., Fernández, J. A., Mato, J. M., Martínez-Chantar, M. L., and Martínez-Cruz, L. A. (2008) *Acta Crystallogr. Sect. F. Struct. Biol. Cryst. Commun.* **64,** 936–941
34. Sharom, F. J., Liu, R., and Romsicki, Y. (1998) *Biochem. Cell Biol.* **76,** 695–708
35. Luckow, V. A., and Summers, M. D. (1988) *Virology* **167,** 56–71
36. Du, K., Sharma, M., and Lukacs, G. L. (2005) *Nat. Struct. Mol. Biol.* **12,** 17–25
37. Grand, T., Mordasini, D., L'Hoste, S., Pennaforte, T., Genete, M., Biyeyeme, M. J., Vargas-Poussou, R., Blanchard, A., Teulon, J., and Lourdel, S. (2009) *Kidney Int.* **76,** 999–1005
38. Piwon, N., Günther, W., Schwake, M., Bösl, M. R., and Jentsch, T. J. (2000) *Nature* **408,** 369–373
39. Jentsch, T. J. (2005) *J. Am. Soc. Nephrol.* **16,** 1549–1561
40. Günther, W., Lüchow, A., Cluzeaud, F., Vandewalle, A., and Jentsch, T. J. (1998) *Proc. Natl. Acad. Sci. U.S.A.* **95,** 8075–8080
41. Elvington, S. M., Liu, C. W., and Maduke, M. C. (2009) *EMBO J.* **28,** 3090–3102

42. Bell, S. P., Curran, P. K., Choi, S., and Mindell, J. A. (2006) *Biochemistry* **45,** 6773–6782
43. He, L., Denton, J., Nehrke, K., and Strange, K. (2006) *Biophys. J.* **90,** 3570–3581
44. Fan, L., Fuss, J. O., Cheng, Q. J., Arvai, A. S., Hammel, M., Roberts, V. A., Cooper, P. K., and Tainer, J. A. (2008) *Cell* **133,** 789–800
45. Shin, D. S., Didonato, M., Barondeau, D. P., Hura, G. L., Hitomi, C., Berglund, J. A., Getzoff, E. D., Cary, S. C., and Tainer, J. A., (2009) *J. Mol. Biol.* **385,** 1534–1555
46. Yamagata, A., and Tainer, J. A. (2007) *EMBO J.* **26,** 878–890
47. Schulz, P., Werner, J., Stauber, T., Henriksen, K., and Fendler, K. (2010) *PLoS One* **5,** e12585